

# Nanocrystalline silicon carbide films for solar photovoltaics: The role of dangling-bond defects\*

Koeng Su Lim<sup>1,‡</sup> and Oleg Shevarevskiy<sup>1,2</sup>

<sup>1</sup>*School of Electrical Engineering and Computer Science, KAIST, Daejeon 307-701, Republic of Korea;* <sup>2</sup>*Solar Energy Conversion Laboratory, Emanuel Institute of Biochemical Physics, Russian Academy of Sciences, Kosygin St. 4, Moscow 119334, Russia*

**Abstract:** Thin films of microcrystalline hydrogenated silicon ( $\mu\text{c-Si:H}$ ) and nanocrystalline silicon carbide ( $\text{nc-SiC:H}$ ) provide a new class of advanced nanostructured materials for solar photovoltaic (PV) devices. We have worked on the fabrication, characterization, and application of these materials for thin film PV solar cells based on amorphous silicon. Here we present an overview of the preparation and characterization methods for heterogeneous SiC:H-based layers. Hydrogenated nc-SiC:H thin film materials with high crystalline volume fraction were deposited using photo-assisted chemical vapor deposition (photo-CVD) technique. The behavior of spin-containing dangling-bond (DB) defects was performed using electron spin resonance (ESR) and transport measurements as a function of sample crystallinity, doping level, and temperature. The electronic and structural properties of intrinsic and doped  $\mu\text{c-Si:H}$  and nc-SiC:H thin films are reviewed with the emphasis of the essential role of DB defects on the photoelectronic transport parameters.

**Keywords:** thin films; nanostructures; semiconductors; photovoltaics; ESR; DB defects.

## INTRODUCTION

The key questions for the next-generation thin film photovoltaic (PV) solar cells based on amorphous silicon are strictly connected with the application of the advanced nanostructured Si-based materials including microcrystalline hydrogenated silicon ( $\mu\text{c-Si:H}$ ) and nanocrystalline silicon carbide ( $\text{nc-SiC:H}$ ) [1–3]. Detailed understanding of structural, electronic, and optical properties is required to provide the adequate recommendations for the growth parameters of such films for PV applications. Over the last few years, extensive research has been provided in order to reach the improved performance of PV devices based on hydrogenated amorphous silicon [4]. Different types of Si–C amorphous thin film materials were successfully used as p-type window layers and the buffer layers in p-i-n junctions [5,6]. The last attempts in this field led to the development of competitive types of hydrogenated nc-SiC:H films with improved photoelectronic parameters [7–9]. It was shown that this kind of layer used as a top-contact p-layer in hydrogenated amorphous silicon n-i-p solar cells improves the cell performance through: (i) the increase of the built-in potential of the top junction; (ii) the improvement of optical transmittance properties; and (iii) the decrease in series resistance [10,11].

---

\*Paper based on a presentation at the International Conference and Exhibition “Molecular and Nanoscale Systems for Energy Conversion” (MEC-2007), 1–3 October 2007, Moscow, Russia. Other presentations are published in this issue, pp. 2069–2161.

‡Corresponding author

To gain high solar cell efficiency, the window layers should have high electrical conductivity, along with wide optical bandgap. Due to C atom incorporation, amorphous a-SiC:H films exhibit higher bandgap compared to a-Si:H but possess low electrical conductivity. The improvement of the electrical properties can be achieved upon doping. However, the process is effective only if the bandgap is lower than 2.1 eV. In nc-SiC:H with higher bandgap value (around 2.5 eV) the doping process is not effective, leaving the dark conductivity not sufficient. The only known possibility of incorporating the high parameters of bandgap and conductivity is to produce the structure consisting of amorphous network with the embedded micro- or nanocrystalline grains. Such inhomogeneous film structure containing crystalline silicon (c-Si) grains and a-SiC:H matrix give rise to a new type of material, hydrogenated nc-SiC:H in which the optical transmittance is governed by a-SiC:H phase while nanocrystalline grains are responsible for the conduction processes.

Phosphorous- or boron-doping considerably enhances nc-SiC:H film conductivity, similarly to what was reported for the doped  $\mu\text{c-Si:H}$  films where the conductivity of  $10^{-1}$  S/cm was observed [12]. At the same time, the doping level may influence the degree of structural disorder, film crystallinity, and defect density distribution. The information about defect densities can be obtained by electron spin resonance (ESR) measurements. ESR techniques have been extensively used for characterizing the neutral Si-related dangling-bond (DB) defects in a-Si:H and  $\mu\text{c-Si:H}$  [13,14]. The ESR signal of the DB defects in a-Si:H shows a width of about 0.1 mT in X-band. In the case of amorphous silicon structures, the ESR signal shows a much broader (2 mT) line with  $g$ -value of 2.008 attributed to inhomogeneous structure. At the same time, little information was available on the paramagnetic state behavior in B-doped nc-SiC:H layers, and there was no clear understanding how the doping process influences the relationship between nc-SiC:H film structure and its crystallinity on one hand and the electronic, optical, and spin-related defects properties on the other.

In our laboratory, we have provided the investigations of intrinsic and B-doped nanocrystalline p-nc-SiC:H films prepared by the mercury (Hg)-sensitized photochemical vapor deposition (photo-CVD) technique using ethylene ( $\text{C}_2\text{H}_4$ ) as a C source. We have also reported on the relationship between film crystallinity, concentration of DB defects, and conductivity [15–17].

The p-nc-SiC:H films were successfully applied as buffer layers for the fabrication of a-Si-based thin film solar cells using the photo-CVD system. For this purpose, using the photo-CVD system we have fabricated the p-i-n-type solar cells with a structure of glass/ $\text{SnO}_2$ /p-a-SiC:H(12 nm)/i-nc-SiC:H(8 nm)/i-a-Si:H(600 nm)/n- $\mu\text{c-Si:H}$ (40 nm)/Al and the area of  $0.09 \text{ cm}^2$  and have investigated their main processing parameters [8,18].

In this lecture, we summarize information on the structural, electronic, and optical properties of nc-SiC:H and nc-SiC:H(B) films providing Raman spectroscopy, ESR, dark conductivity, and optical absorption measurements. We emphasize the role of DB defects in the main photoelectronic parameters of the materials under consideration.

## PHOTO-ASSISTED CHEMICAL VAPOR DEPOSITION PROCESS

To get an adequate understanding of the behavior of thin film materials under consideration, we have prepared several sets of intrinsic, nc-SiC:H, and boron-doped (B-doped), nc-SiC:H(B) hydrogenated films that have been grown in a Hg-sensitized photo-CVD system using the mixture of silane ( $\text{SiH}_4$ ), hydrogen ( $\text{H}_2$ ), diborane ( $\text{B}_2\text{H}_6$ ), and ethylene ( $\text{C}_2\text{H}_4$ ) reactant gases on glass substrates. To dissociate the gas mixture, a low-pressure Hg lamp emitting 184.9- and 253.7-nm resonance lines was used as an ultraviolet (UV) light source. Since photo-CVD is a sufficiently soft process (the applied power was about  $10 \text{ mW/cm}^2$ ), the damage of the film surface by the ions was negligible. The detailed description of the deposition process can be found in our previous publications [19,20]. Several sets of intrinsic and B-doped samples, some with a varied doping level, and some with a constant doping level but with varied C-content, were prepared. During the deposition of the intrinsic samples, the hydrogen dilution ratio

( $H_2/[SiH_4]$ ), ethylene gas flow ratio ( $[C_2H_4]/[SiH_4]$ ), chamber pressure, mercury bath temperature, and substrate temperature were normally kept at 20, 0.07, 0.46 torr, and 20 and 250 °C, respectively. The B-doping level in p-nc-SiC:H films was proportional to  $B_2H_6$  gas flow ratio,  $[B_2H_6]/[SiH_4]$ , and varied from 0 to 8000 ppm. Under similar growth conditions, a set of samples was also prepared with a constant (3000 ppm) doping level while the C-content varied from 5 to 11 at. %.

## METHODS FOR CHARACTERIZATION OF THIN FILM LAYERS

The films with a thickness of around 150 nm were deposited onto Corning 7059 glass substrates for optoelectronic and ESR measurements. The structural properties of the films were controlled by X-ray diffraction (XRD) and Raman spectroscopy measurements in the range 400–600  $cm^{-1}$ . The nominal C-content in the nc-SiC:H film was proportional to the controlled parameter of the flow rate of  $C_2H_2$  and  $SiH_4$  reactant gases.

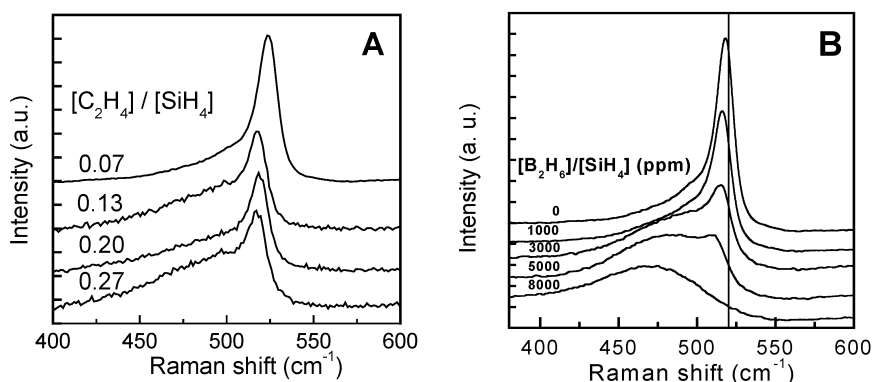
To provide the electrical conductivity measurements, a planar gap-cell configuration with vacuum-evaporated Al contacts was used. The temperature dependence of dark conductivity was measured in the temperature range 300–420 K. During the measurements, the Ohmic nature of contacts was established by the behavior of the current–voltage ( $I$ – $V$ ) curves. The conductivity of the films was determined from the  $I$ – $V$  characteristics using a semiconductor parameter analyzer. The value of optical gap  $E_{04}$  was extracted from optical absorption measurements.

The ESR spectra were recorded using a standard X-band ESR spectrometer with  $TM_{011}$  mode cavity operating at 9.6 GHz microwave frequency. The magnetic field modulation frequency was 100 kHz. The  $g$ -values were determined by measuring the difference between resonance peak and that of a signal with a known  $g$ -value from  $Mn^{2+}$ -containing probe. The absolute spin densities were calculated by comparing the doubly integrated values of the signal with a known paramagnetic standard. No ESR signal was detected from Corning glass substrates. The detectable limit for 100-nm-thick layers of a standard sample with an area of  $0.5 \times 1 \text{ cm}^2$  was estimated to be around  $2 \times 10^{17}$  spins/ $cm^3$ .

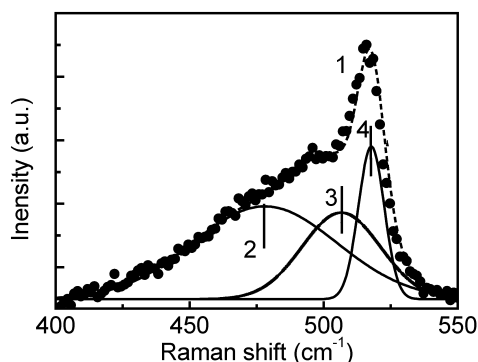
## STRUCTURAL PROPERTIES OF HETEROGENEOUS FILMS

Figure 1A shows the evolution of Raman spectra in a set of intrinsic hydrogen-diluted ( $H_2/[SiH_4] = 20$ ) nc-SiC:H films deposited under varied gas flow ratio  $[C_2H_4]/[SiH_4]$ . Raman spectra presented in Fig. 1B show an appropriate data for a set of B-doped nc-SiC:H(B) films deposited at different ratios of  $[B_2H_6]/[SiH_4]$  and at constant gas flow ratio  $[C_2H_4]/[SiH_4] = 0.07$ , which corresponds to the C-content of ~1 at. % as was obtained from Auger measurement. The analysis of all Raman spectra were provided by decomposing the experimental curve into three components found near 520, 480, and 500–506  $cm^{-1}$ , which corresponds, respectively, to c-Si, a-Si:H, and an additional intermediate fraction associated with bond dilation at grain boundaries (GBs) [21,22]. Figure 2 gives an example of how the mentioned decompositions were provided for the case of the intrinsic nc-SiC:H film prepared under  $[C_2H_4]/[SiH_4]$  gas flow ratio, equal to 0.13 (see Fig. 1A).

It is known that in a-SiC:H amorphous layers with low C-content, the broad peak exhibited near 480  $cm^{-1}$  has a negligible deviation from the a-Si:H peak and cannot be resolved. The existence of Si–C bonds in the films under investigation was proved by Fourier transform infrared (FTIR) measurements. Meanwhile, no Raman peak associated with the c-SiC phase was observed in the range of 750–950  $cm^{-1}$ . The presence of c-Si grains was confirmed by XRD data that have shown the peaks corresponding to  $\langle 111 \rangle$ ,  $\langle 220 \rangle$ , and  $\langle 311 \rangle$  planes of c-Si. The average size of crystalline grains as deduced from full width at half maximum (FWHM) using the Scherrer formula [23] was found to be around 12 nm.



**Fig. 1** Raman scattering spectra for: (A) intrinsic nc-SiC:H films prepared under varied value of [C<sub>2</sub>H<sub>4</sub>]/[SiH<sub>4</sub>] gas flow ratio, and (B) B-doped nc-SiC:H films prepared by photo-CVD with boron gas doping ratio [B<sub>2</sub>H<sub>6</sub>]/[SiH<sub>4</sub>] varying from 0 to 8000 ppm.



**Fig. 2** Decomposition of the experimental Raman scattering spectra (1) into three Raman modes centered at (2), (3), and (4) position for intrinsic nc-SiC:H film prepared under [C<sub>2</sub>H<sub>4</sub>]/[SiH<sub>4</sub>] = 0.13.

Following [22], the crystalline volume fraction,  $X_C$ , was determined from the Raman peaks intensity ratio with a correction to nanoscale size of the crystalline grains

$$X_C(\%) = \frac{I_{520} + I_{506}}{I_{520} + I_{506} + y(L)I_{480}} \times 100 \quad (1)$$

where  $I_{520}$ ,  $I_{506}$ , and  $I_{480}$  are, respectively, integrated intensities of the appropriate Raman modes, and  $y(L)$  is a prefactor varying with the grain size  $L$  (given in nm) and calculated as  $y(L) = 0.1 + \exp[-(L/25)]$  [24].

Appropriately, the volume fraction of GB phase, associated with 506 cm<sup>-1</sup> peak position,  $X_{GB}$ , was deduced as follows:

$$X_{GB}(\%) = \frac{I_{506}}{I_{520} + I_{506} + y(L)I_{480}} \times 100 \quad (2)$$

The evolution of Raman spectra presented in Fig. 1A demonstrates the changes in nc-SiC:H structure with the increase of C-content gained with the enhancement of [C<sub>2</sub>H<sub>4</sub>]/[SiH<sub>4</sub>] gas flow ratio during deposition. It is seen that with the C-content increase, the sharp peak at ~520 cm<sup>-1</sup> diminishes, while a broad line of amorphous phase positioned at ~480 cm<sup>-1</sup> becomes more intensive. The crystalline vol-

ume fraction  $X_C$  and  $X_{GB}$  fraction estimated using formulas 1 and 2 is plotted in Fig. 3 vs.  $[C_2H_4]/[SiH_4]$ . The deposition provided under the lowest value of  $[C_2H_4]/[SiH_4] = 0.07$  produces highly crystalline film ( $X_C = 86\%$ ), while the increase of C-content ( $[C_2H_4]/[SiH_4] > 0.1$ ) results in formation of a predominantly disordered structure.

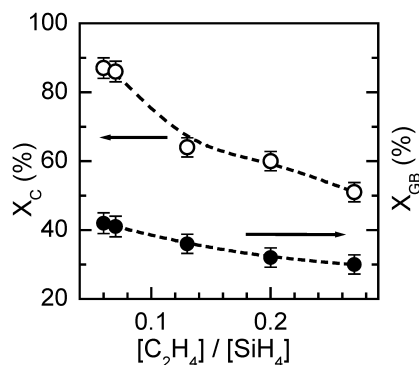


**Fig. 3** Volume fraction content of  $X_C$  and  $X_{GB}$ , for nc-SiC:H films as a function of  $[C_2H_4]/[SiH_4]$  gas flow ratio. Dashed lines are drawn to guide the eye.

The evolution of Raman spectra given in Fig. 1B indicates the transition from nanocrystalline to amorphous structure. The increase in B-doping level causes the broadening and diminishing of the sharp peak at  $\sim 520\text{ cm}^{-1}$ , while a broad line of amorphous phase positioned at  $\sim 480\text{ cm}^{-1}$  becomes more intensive.

The behavior of the nanocrystalline volume fraction  $X_C$  for B-doped nc-SiC:H(B) films is shown in Fig. 4 as a function of  $[B_2H_6]/[SiH_4]$  gas doping ratio. It can be concluded that, starting from a highly crystalline film content of  $X_C = 67\%$  (undoped sample), the increase in  $[B_2H_6]/[SiH_4]$  induces the reduction of film crystallinity. Our studies revealed that at low doping levels ( $[B_2H_6]/[SiH_4] < 4000\text{ ppm}$ ), the samples possess inhomogeneous structure consisting of nc-Si grains and amorphous matrix. At gas doping ratios of 4000 ppm and higher, the portion of the amorphous fraction dominates, and, finally, in 8000 ppm B-doped sample no trace of crystallinity is detected.

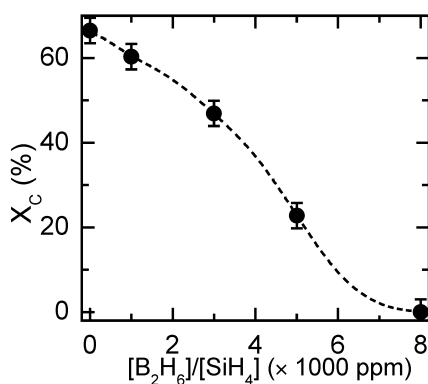


**Fig. 4** Nanocrystalline volume fraction content ( $X_C$ ) for B-doped nc-SiC:H(B) films as a function of boron gas doping ratio  $[B_2H_6]/[SiH_4]$ .

## ELECTRONIC PROPERTIES AND DANGLING-BOND DEFECTS

The density of paramagnetic defects and the electronic properties of nc-SiC:H films depend on both the film crystallinity and the C-content. The evolution of room-temperature ESR spectrum of nc-SiC:H films with different C-content is given in Fig. 5. All the samples demonstrate slightly unsymmetrical single broad ESR line with a peak-to-peak width ( $\Delta H_{pp}$ ) of around 20–30 G and the  $g$ -value of 2.0065 ( $\pm 0.0005$ ), which is assigned to neutral DB defects. The spin density of DB states for highly crystalline sample was found to be around  $10^{19} \text{ cm}^{-3}$ , while the film with low crystalline content ( $X_C = 51\%$ ) demonstrates an order of magnitude lower value of  $2.8 \times 10^{18} \text{ cm}^{-3}$ .

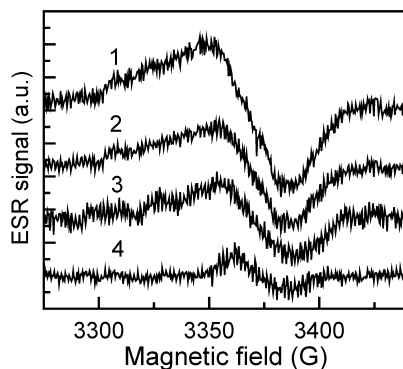


**Fig. 5** The evolution of room-temperature ESR spectrum for a set of nc-SiC:H films with crystalline fraction content decreasing from sample 1 ( $X_C = 86\%$ ) to 4 ( $X_C = 51\%$ ).

In Fig. 6, the DB density in nc-SiC:H films is plotted as a function of  $[\text{C}_2\text{H}_4]/[\text{SiH}_4]$ . An additional point belongs to highly crystalline film with  $N_S = 6 \times 10^{19} \text{ cm}^{-3}$  prepared under increased hydrogen dilution ratio ( $\text{H}_2/[\text{SiH}_4] = 25$ ). The enhancement of the C-content during nc-SiC:H film growth seems to hinder the formation of the crystalline phase. As a result, the defect concentration and the film conductivity decrease considerably. Figure 7 shows the behavior of the room-temperature dark conductivity ( $\sigma_D$ ) for the samples with different C-content. The sample with small C-content prepared under  $[\text{C}_2\text{H}_4]/[\text{SiH}_4] = 0.07$  ( $X_C = 86\%$ ) shows a maximum conductivity of  $3.8 \times 10^{-6} \text{ S/cm}$ . The C-content increase decreases the value of  $X_C$ . Along with it,  $\sigma_D$  also decreases to the value of  $\sigma_D = 3.2 \times 10^{-8} \text{ S/cm}$  for  $X_C = 51\%$ . It is obvious that the high conductivity in nc-SiC:H films is gained due to the high crystalline fraction content in accordance with similar results reported in [13].

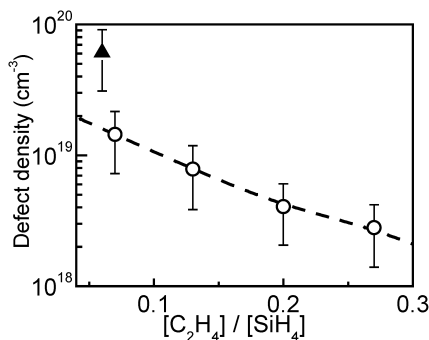


**Fig. 6** Spin defect density,  $N_S$ , extracted from ESR spectra of nc-SiC:H films as a function of  $[\text{C}_2\text{H}_4]/[\text{SiH}_4]$  gas flow ratio (circles). An additional point (triangle) belongs to a sample prepared under higher hydrogen dilution. The dashed line is drawn to guide the eye.

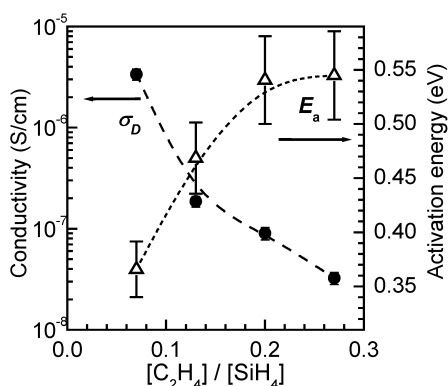


**Fig. 7** Room-temperature dark conductivity ( $\sigma_D$ ) and activation energy ( $E_a$ ) of nc-SiC:H films, as a function of  $[\text{C}_2\text{H}_4]/[\text{SiH}_4]$  gas flow ratio. The dashed lines are drawn to guide the eye.

In the temperature range of 300–420 K, the films under consideration demonstrated the linear dependence of conductivity on the reversed temperature. Figure 6 shows the values of activation energy ( $E_a$ ) extracted from the Arrhenius plots of  $\sigma_D$  using the known equation

$$\sigma_D = \sigma_0 \exp(-E_a/kT) \quad (3)$$

where  $\sigma_0$  is the conductivity prefactor. It is seen that  $E_a$  is small in predominantly crystalline layers with high conductivity. We may also conclude that in the temperature range of our investigations, the nc-SiC:H films demonstrate thermally activated transport mechanism.

The densities of paramagnetic defects and the electronic properties of both intrinsic and B-doped nc-SiC:H films appear to demonstrate a very similar behavior. At the same time, in B-doped nc-SiC:H(B) samples, the intensity of the ESR line (proportional to the concentration of DB defects) depends not only on film crystallinity and C-content, but also on the doping level. The evolution of the room-temperature ESR spectrum with doping in nc-SiC:H(B) films ( $[\text{C}_2\text{H}_4]/[\text{SiH}_4] = 0.07$ ) is given in Fig. 8. The samples demonstrate an unsymmetrical single broad ESR line with a peak-to-peak width ( $\Delta H_{pp}$ ) of around 20–30 G and a  $g$ -value of 2.0065 ( $\pm 0.0005$ ), which is also assigned to neutral silicon DB defects.

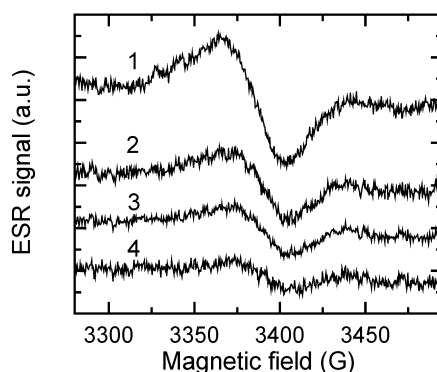


**Fig. 8** The evolution of room-temperature ESR spectrum for a set of nc-SiC:H(B) films with increasing (from 1 to 4 spectra) the doping level from 1000 to 8000 ppm.

Figure 9 provides the illustration of the influence of B-doping on the spin densities ( $N_S$ ) and dark conductivities ( $\sigma_D$ ) in nc-SiC:H(B) films. The enhancement of doping level seems to provide an equal effect on film crystallinity compared with the enhancement of C-content in the undoped nc-SiC:H films, both hindering the formation of the crystalline phase during the film growth. It is seen that at low gas doping ratios the B-doping initiates the increase of room-temperature dark conductivity from  $8.6 \times 10^{-8}$  S/cm to a maximum of  $5.5 \times 10^{-2}$  S/cm for 3000-ppm doped film. The further increase in  $[B_2H_6]/[SiH_4]$  gives rise to a rapid decrease in  $\sigma_D$  down to the value of  $3.1 \times 10^{-6}$  S/cm for the 8000-ppm doped film. The spin defect density in the 1000-ppm B-doped sample is around  $10^{19}$  cm $^{-3}$ , while the further increase in B-doping is accompanied by a strong decrease of  $N_S$  to a value of  $9 \times 10^{17}$  cm $^{-3}$ .

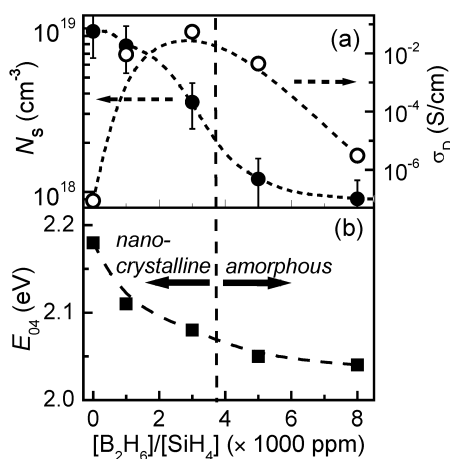


**Fig. 9** Spin defect density,  $N_S$ , room-temperature dark conductivity  $\sigma_D$  (a), and  $E_{04}$  optical bandgap (b) of B-doped nc-SiC:H(B) films as a function of boron gas doping ratio  $[B_2H_6]/[SiH_4]$ .

The behavior of both  $\sigma_D$  and  $N_S$  values with doping reflects the nanocrystalline to amorphous structure transition caused by the decrease of film crystallinity. It thus becomes obvious that the increase in  $\sigma_D$  with doping in nc-SiC:H(B) films can only be gained in highly crystalline samples in accordance with similar results reported in [9]. It was found that B-doping also influences the optical absorption properties of silicon carbide films. The appropriate behavior of the  $E_{04}$  optical gap extracted from SE measurements is given in Fig. 9b. The decrease of  $E_{04}$  with B-doping follows a similar behavior observed in SiC:H films.

In order to clarify the DB behavior in B-doped films, we have prepared and investigated an additional set of samples with varied C-content. The carbon incorporation in nc-SiC:H films was proportional to the  $[C_2H_4]/[SiH_4]$  ratio that varied during film growth between 0 and 0.27. Figure 9 shows the evolution of room-temperature ESR spectrum for 3000-ppm B-doped nc-SiC:H films with the increase of C-content. From the inset in Fig. 10, it can be clearly seen that spin defect density increases with the increase of the C-content. In this particular case, the increase of DB concentration is observed for the samples with mainly amorphous structure and can be explained by the creation of additional C-related spin defects that were previously reported in [14].

The shape and the position of ESR lines observed in our studies originate from c-Si GB defects and the specific orientation of crystallites grown [14]. Very similar ESR signals with the  $g$ -factor ranging from 2.005 to 2.01,  $\Delta H_{pp} \sim 20$  G and DB spin densities  $N_S \sim 10^{17}$ – $10^{19}$  cm $^{-3}$  have been reported for intrinsic and doped  $\mu$ c-SiC:H samples prepared by the plasma-enhanced chemical vapor deposition (PECVD) technique [25].

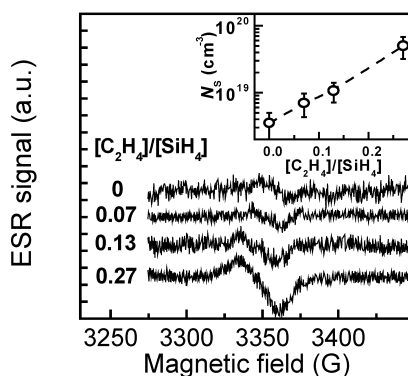


**Fig. 10** Evolution of room-temperature ESR spectrum for 3000-ppm B-doped *nc*-SiC:H films with the increase of C-content proportional to the ethylene gas flow ratio  $[C_2H_4]/[SiH_4]$ . In the inset,  $N_S$  is plotted as a function of  $[C_2H_4]/[SiH_4]$  ratio.

The increase of B-doping initiates the structural changes from crystalline to amorphous growth when the gas doping ratio reaches the value of around 3000–4000 ppm. The dashed line in Fig. 9 indicates an approximate position of the transition from crystalline to amorphous film growth. To the left of a dashed line with the nanocrystalline growth regime, the dark conductivity increases with doping. To the right of the dashed line, the portion of the amorphous fraction dominates and the conductivity drops with the decrease of crystalline content. After the transition to the amorphous growth, the increase of B-doping level does not increase the film conductivity. However, the samples with poor crystallinity possess a certain amount of GB fraction that can be responsible for high defect density and the increased values of conductivity. Along with the increase of the C-content in the samples with low crystallinity,  $N_S$  concentration was found to also increase due to the creation of an additional amount of C-related defects.

The broadening of the ESR lines observed for all the films can be ascribed to the large distribution of DB states in crystalline fraction [24], while the peak position may be influenced by the orientation of crystalline grains in the bulk of the film that give rise to a high  $g$ -factor anisotropy. Similar behavior of the  $g$ -factor was observed in  $\mu c$ -Si:H films [26,27]. In thin ( $\sim 100$  nm) films, the line broadening may also originate from surface-related spin defects. Thus, for a-Si:H film, it was shown [28] that defects with a surface spin density of around  $10^{13}$  spins/cm<sup>2</sup> are distributed into the bulk of the film at 100 nm depth.

The increase of C-concentration in a-SiC:H films is known to produce samples with high  $N_S$  due to the creation of C-related DB [25]. However, the data given in Figs. 6 and 9a demonstrate quite an opposite behavior that needs to be explained. The point is that the defect density in *nc*-SiC:H films is proportional to the different parameters: film crystallinity and C-content. The reduction of crystalline phase decreases the defect density due to diminishing of the amount of DB defects related to c-Si grains. At the same time, such a decrease of film crystallinity was initiated by the increase of C-content. In parallel with this, the increase of C-content produces an additional amount of defects.

We assume that the increase of C-content during the film growth accompanied by the creation of additional C-related DB defects slightly increases the total  $N_S$  value. However, along with it, the enhancement of C-concentration diminishes the content of both the crystalline and GB fractions, resulting in comparatively strong decrease of Si-related DB defects. As a result, the ESR measurements reveal that in hydrogen-diluted *nc*-SiC:H samples, the amount of created paramagnetic defects is mainly effected by film crystallinity while the impact of C-related defects is much lower. The observed behavior is in accordance with similar data reported in [14] for PECVD deposited intrinsic  $\mu c$ -Si:H layers where the enhancement of DB density was observed with increasing the film crystallinity. For the case

of nc-SiC:H and nc-SiC:H(B) films, we may assume that during the photo-CVD growth the enhancement of C-containing reactant gas hinders the process of nanocrystalline fraction creation.

To conclude, the above examples serve to illustrate the fact that the concentrations of DB defects in heterogeneous nanocrystalline Si-based thin film materials play an important role in electrical conductivity processes, while the impact of DB states in charge-transfer mechanism can be completely different in comparison with that observed in Si-based bulk materials.

## ACKNOWLEDGMENTS

One of the authors (O. Sh.) is grateful to the Russian Foundation for Basic Research (RFBR) for a partial supporting of this work by RFBR Grant No. 07-08-00363-a.

## REFERENCES

1. Y. Hamakawa, H. Okamoto, Y. Tawada. *Int. J. Sol. Energy* **1**, 125 (1982).
2. Y. Tawada, K. Tsuge, M. Kondo, H. Okamoto, Y. Hamakawa. *J. Appl. Phys.* **53**, 5273 (1982).
3. S. Y. Myong, H. K. Lee, E. Yoon, K. S. Lim. *J. Non-Cryst. Solids* **298**, 131 (2002).
4. S. Guha. *J. Non-Cryst. Solids* **198–200**, 1076 (1996).
5. K. S. Lim, M. Konagai, K. Takahashi. *J. Appl. Phys.* **56**, 538 (1984).
6. W. Y. Kim, H. Tasaki, M. Konagai, K. Takahashi. *J. Appl. Phys.* **61**, 3071 (1987).
7. C. H. Lee, J. W. Jeon, K. S. Lim. *J. Appl. Phys.* **87**, 8778 (2000).
8. S. Y. Myong, T. H. Kim, K. S. Lim, K. H. Kim, B. T. Ahn, S. Miyajima, M. Konagai. *Sol. Energy Mater. Sol. Cells* **81**, 485 (2004).
9. S. Y. Myong, S. S. Kim, K. S. Lim. *J. Appl. Phys.* **95**, 1525 (2004).
10. G. M. Ferreira, C. Chen, R. J. Koval, J. M. Pearce, C. R. Wronski, R. W. Collins. *J. Non-Cryst. Solids* **338–340**, 694 (2004).
11. S. Guha, J. Yang, P. Nath, M. Hack. *Appl. Phys. Lett.* **49**, 218 (1986).
12. A. Dasgupta, S. Ghosh, S. Ray. *J. Mater. Sci. Lett.* **14**, 1037 (1995).
13. R. Schropp. *Thin Solid Films* **403–404**, 17 (2002).
14. A. L. Baia Neto, A. Lambertz, R. Carius, F. Finger. *Phys. Status Solidi* **186**, R4 (2001).
15. O. Chevaleevski, S. Y. Myong, K. S. Lim. *Solid State Commun.* **128**, 355 (2003).
16. O. I. Shevaleevskii, A. A. Tsvetkov, L. L. Larina, S. Y. Myong, K. S. Lim. *Semiconductors* **38**, 528 (2004).
17. O. I. Shevaleevskiy, S. Y. Myong, K. S. Lim, S. Miyadjima, M. Konagai. *Semiconductors* **39**, 709 (2005).
18. S. Y. Myong, K. S. Lim. *Appl. Phys. Lett.* **86**, 1 (2005).
19. J. H. Yang, K. S. Lim. *Appl. Phys. Lett.* **71**, 1846 (1997).
20. J. W. Lee, K. S. Lim. *Appl. Phys. Lett.* **68**, 1031(1996).
21. D. Han, G. Yue, J. D. Lorentzen, J. Lin. *J. Appl. Phys.* **87**, 1882 (2000).
22. S. Veprek, F. A. Sarott, Z. Iqbal. *Phys. Rev. B* **36**, 3344 (1987).
23. Z. Iqbal, S. Veprek. *J. Phys. C* **15**, 377 (1982).
24. E. Bustarret, M. A. Hachicha, M. Brunel. *Appl. Phys. Lett.* **52**, 1675 (1988).
25. F. Demichelis, C. F. Pirri, E. Tresso. *J. Appl. Phys.* **72**, 1327 (1982).
26. X. Liu, G. Xu, Y. Sui, Y. He, X. Bao. *Solid State Commun.* **119**, 397 (2001).
27. F. Finger, J. Muller, C. Malten, R. Carius, H. Wagner. *J. Non-Cryst. Solids* **266–269**, 511 (2000).
28. U. K. Das, T. Yasuda, S. Yamasaki. *Phys. Rev. Lett.* **85**, 2324 (2000).